IEEE Open Journal of
Circuits and Systems

Received 5 July 2020; revised 22 September 2020 and 28 October 2020; accepted 31 October 2020. Date of current version 10 December 2020.

Digital Object Identifier 10.1109/OJCAS.2020.3035771

Efficient Design of Zero-Phase Riesz Fractional Order Digital Differentiator Using Manta-Ray Foraging Optimisation for Precise Electrocardiogram QRS Detection

CHANDAN NAYAK [1], SUMAN KUMAR SAHA [1], RAJIB KAR [2] (Senior Member, IEEE), AND DURBADAL MANDAL [2] (Member, IEEE)

[1]Department of ECE, NIT Raipur, Raipur 492010, India

[2]Department of ECE, NIT Durgapur, Durgapur 713209, India

This article was recommended by Associate Editor M. Tavakoli-Kakhki.

CORRESPONDING AUTHOR: C. NAYAK (e-mail: chandanayak234@gmail.com)

This work was supported by Science and Engineering Research Board, Department of Science and Technology, Government of India under Grant EEQ/2016/000215.

This article has supplementary downloadable material available at https://doi.org/10.1109/OJCAS.2020.3035771, provided by the authors.

ABSTRACT This article introduces a new design of an optimised zero-phase response fractional order digital differentiator (FODD) called Riesz FODD of half order by employing a recently developed Manta-Ray Foraging Optimisation (MRFO) for improved and precise electrocardiogram QRS detection. A new weighted cost function is developed that precisely considers the characteristics of an ideal Riesz fractional-order differentiator. Simulation tests of the rational approximations of the Riesz FODD based on the MRFO algorithm ensure close correspondence with the theoretical zero-phase and near-ideal magnitude responses and sensibly supersede the Least-squares method, Convex optimisation, Flower Pollination Algorithm, and Artificial Bee Colony based Riesz FODD designs. The Zero-phase response of the proposed Riesz FODD assists in preserving the features of the differentiated ECG precisely at the same time instant where they occur in the unfiltered signal. Additionally, the optimal magnitude characteristics of the proposed Riesz FODD help to obtain highly accurate differentiated ECG. These two indigenous properties of the proposed Riesz FODD accommodate the QRS detector to precisely identify the R-peak location and thus sensibly escalate the QRS detection accuracy when tested against several real electrocardiogram (ECG) signals of the PhysioNet ECG repository.

INDEX TERMS ECG, FIR filter, fractional order Riesz digital differentiator, Manta-Ray foraging optimisation, zero-phase.

I. INTRODUCTION

ELECTROCARDIOGRAM (ECG) signal analysis, especially QRS complex detection, has been intensively investigated by several research communities for more than the last three decades [1]. It has become more ubiquitous in recent times due to its popular demand in a cardiac care centre for the prompt and detailed examination of the large quantity of ECG signals. The automatic ECG analysis algorithms minimise the overall workload of the cardiologists. Precise measurement of R-peak location is considered to be the basis of the diagnosis of several types of heart ailments, such as myocardial infarction, heart-rate turbulence, sleep apnoea, and abnormal heartbeat rhythm [1]. In this context, reliable and precise detection of R-peak locations by the automatic QRS detector plays a vital task in accurate diagnosis and early intervention of cardiovascular diseases (CVDs).

In literature, the QRS complex detectors are implemented by employing several techniques, such as wavelet transform [2], adaptive linear predictor preceded by

Savitzky-Golay filter [3], two-stage median filter and peak enhancement [4], phase portraits and box-scoring [5], parallel delta modulator [6], relative energy-based nonlinear filtering [7], total variation denoising [8], maximum-minimum difference curve generation [9], event-related moving average filter [10], signal structural analysis [11], R-R interval assessment method [12], Hilbert transform (HT) [13], etc.

Out of various R-peak detection techniques reported in [2]–[13], the differentiator based R-peak detection approach is more prevalently employed in real-time QRS complex detection methods, due to its benefits like (i) computational efficiency, and (ii) independent of algorithm's training, patient, and manual segmentation of ECG signal [1]. In the reported differentiator based QRS detection approaches, both integer order differentiator (IOD) [14]–[16] and fractional order differentiator (FOD) [17]–[19] have been employed to generate QRS related feature signal. The produced QRS feature signal is the input to the peak detection block. The QRS complex is detected by employing either threshold independent or thresholding based peak detection logic.

From literature, it has been ensured that compared to the integer order calculus, more details of the signal can be effectively preserved by the fractional order calculus [17]–[19]. The integer order derivative, $D^n x(t) = d^n x(t)/dt^n$ is generalised to fractional-order derivative, $D^p x(t) = d^p x(t)/dt^p$ to achieve enhanced accuracy and flexibility in the design. Here, n and p represent integer number and real number, respectively. The IOD is regarded as a particular case of FOD for $p = 1$. Thus, compared to IOD based QRS complex detectors [14]–[16], superior QRS complex detection performance is obtained for the fractional-order digital differentiator (FODD) based QRS detector [19].

Considering wide applications of FODD, numerous FODD design methodologies have been published. A comprehensive exposition of all of the advanced FODD design approaches can be found in [20].

All those above mentioned conventional FODD design approaches [17]–[19] are designed by using (1).

$$H_i(\omega) = (j\omega)^p \tag{1}$$

where p is the order of the FODD and ω denotes the digital frequency normalised to [0, 1].

Equation (1) denotes the frequency response (FR) of the ideal FODD, which provides a constant $(p\pi/2)$ phase response. When a complex nature signal, which is the mixture of signals of different frequencies and phase shifts, is passed through an ideal differentiator, each phase shift components of the signal is shifted by $(p\pi/2)$ amount. However, in realistic differentiator design, the ideal phase response of the realised differentiator can never be achieved. As a result of this, in the differentiated signal, the correct harmony among different frequency components is disturbed due to the uncontrolled phase response of the realistic differentiator. To overcome the cited problem, an optimally designed differentiator with its zero-phase response characteristic called Riesz FODD is proposed, mitigating the uncontrolled phase shift problem to a great extent.

The FR of the ideal zero-phase response FODD is defined in (2).

$$G_i(\omega) = |\omega|^p \tag{2}$$

The FODD with the zero-phase response is called as Riesz FODD because it is related to the Riesz potential. Despite many advantages of the Riesz FODD, only a few researchers have developed it in existing literature [21]–[23] so far. In [21], firstly, the analytical methods such as Tustin's, fractional differencing (FD), and discrete cosine transform (DCT) are used to design conventional differentiators. Next, the FRs of the designed differentiators are employed to realise Riesz FODDs. Similarly, to realise the Riesz FODD, the FR of the analytical discrete sine transform (DST) based differentiator is employed in [22]. In [23], the digital image is sharpened by using Riesz FODD together with discrete Hartley transform. In [24], the locations of ECG QRS complexes are identified by adopting analytical FD based Riesz FODD. However, the optimally designed Riesz FODD provides an improved FR compared to the analytical method based designs. Thus, the subsequent application of the optimally designed Riesz FODD on biomedical signal processing, especially on ECG QRS complex detection is more beneficial, which is yet to be studied. This has encouraged the authors to explore this research area.

The reported Riesz FODDs [21]–[24] are designed by adopting conventional gradient-based analytical methods. As the major problem associated with the Riesz FODD design problem lies in its multimodal, multidimensional, nonuniform, nonlinear, and non-differentiable nature error function, so the final solution obtained by the reported analytical methods based Riesz FODD designs [21]–[24] do not converge to the global optimum as discussed in sections to follow. To combat this difficulty, an effective evolutionary algorithm (EA) such as Manta-Ray Foraging Optimisation (MRFO) [25] based one-step method to realise the Riesz FODD is firstly proposed in this article. Subsequently, its real-time application on ECG QRS complex detection is also examined, as discussed in subsequent sections. In the following points, the critical contributions of this article are highlighted: (i) Several FIR-type $N = 22$nd order Riesz FODD models for fractional order, $p = 1/2$ are realised by employing classical optimisation methods, such as Least-squares (LS) method [26] and Convex optimisation (CVXO) [27] along with the nature-inspired evolutionary techniques, such as Artificial Bee Colony (ABC) [28], Flower Pollination Algorithm (FPA) [29], and MRFO; (ii) A new and practical application of the MRFO-based Riesz FODD is demonstrated by employing it in the pre-processing stage of a recently proposed QRS complex detector [19]; and (iii) The

performance of the MRFO Riesz FODD based QRS complex detector is authenticated against benchmark MIT/BIH Noise Stress Test database (NSTDB), European ST-T database (EDB), MIT/BIH Arrhythmia Database (MITDB), MIT/BIH Supraventricular Arrhythmia database (SVDB), Atrial Fibrillation Termination Challenge database (AFTDB), and T-Wave Alternans Challenge Database (TWADB) ECG records to show its broad sense of precise QRS detection capability.

II. RIESZ FRACTIONAL-ORDER DIFFERENTIATOR

In the continuous-time domain, the Riesz FOD is presented below.

The Riesz kernel is obtained by estimating the inverse Fourier transform (FT) of (2) and is presented in (3) [21].

$$K(t) = \left[1/\{2\Gamma(-p)\cos(p\pi/2)\}\right] \times |t|^{-p-1} \tag{3}$$

where $\Gamma(\cdot)$ is the gamma function.

The Riesz kernel is applied to calculate the pth order Riesz FOD of signal $x(t)$ and is shown in (4) [21].

$$D^p x(t) = K(t) * x(t) \tag{4}$$

$$D^p x(t) = \left[1/\{2\Gamma(-p)\cos(p\pi/2)\}\right] \int_{-\infty}^{\infty} |t-\tau|^{-p-1} x(\tau) d\tau \tag{5}$$

Equation (6) is used to find the FT of (5).

$$\mathrm{FT}\left[D^p x(t)\right] = |\omega|^p X(\omega) \tag{6}$$

where $X(\omega)$ represents the FT of $x(t)$.

The Riesz differentiator proposed by Tseng and Lee [21] is given in (7). It states that if the FR of the designed conventional differentiator, $H_d(\omega)$ closely approximates the FR of its ideal differentiator counterpart, $H_i(\omega)$, then only the $G_{dt}(\omega)$ of the designed digital Riesz FOD closely approximates to its ideal Riesz FOD, $G_i(\omega)$.

$$G_{dt}(\omega) = [H_d(\omega) + H_d(-\omega)]/2\cos(p\pi/2) \tag{7}$$

It is worth mentioning that if the designed conventional differentiator's FR, $H_d(\omega)$ is purely ideal and the mathematical relationship, as given in (7), is followed, then the FR of the designed Riesz differentiator will closely approximate the FR of its ideal differentiator counterpart [21]. However, it is not possible to retain an ideal differentiator response due to its size limitation. For this reason, instead of having an ideal zero-phase and an ideal magnitude response (MR), a very close approximation to those characteristics can only be achieved with an adequately formulated objective function and an efficiently chosen metaheuristic optimisation algorithm with suitable control parameters as discussed in next sections.

III. PROBLEM STATEMENT

An N^{th} order FIR-type Riesz FODD is defined in (8).

$$H_d(Z) = \sum_{n=0}^{N} h(n) z^{-n} \tag{8}$$

where $h(n)$ for $n = 0, 1, 2, 3, \ldots, N$, are the coefficients of $H_d(Z)$.

The corresponding FR of $H_d(Z)$ is defined in (9).

$$H_d(\omega) = \sum_{n=0}^{N} h(n)\, e^{-j\omega n} \tag{9}$$

The proposed FIR-type Riesz FODD design methodology, as shown in Fig. 1, is articulated as an approximation problem. Here the FR of the proposed Riesz FODD, $G_{dprop}(\omega)$ closely approximates the FR of the ideal zero-phase response differentiator, $G_i(\omega)$ by employing the optimisation techniques. Four steps are involved in designing the Riesz FODD coefficients: (a) define the FR of ideal zero-phase response differentiator, $G_i(\omega)$ and calculate its MR $|G_i(\omega)|$, (b) randomly distribute $((N/2)+1)$ coefficients of $H_d(Z)$ in search space; find $H_d(Z^{-1})$, and form Nth order Riesz FODD $G_{dprop}(z) = (H_d(z) + H_d(z^{-1}))/2\cos(p\pi/2)$; calculate its magnitude $|G_{dprop}(\omega)|$ and phase $\angle G_{dprop}(\omega)$ responses, (c) properly design an optimality criterion (J_{DD} as defined in (10)) to minimise the FR error between $G_{dprop}(\omega)$ and $G_i(\omega)$, and (d) apply suitable optimisation methods with the best control variables to optimise the Riesz FODD coefficients.

$$J_{DD} = (w \times E_{\max}) + [(1-w) \times E_{sum}] + \left[w \times T_{phase}\right] \tag{10}$$

where maximum error $E_{max} = \max(E_m)$; here $E_m = ||G_i(\omega)| - |G_{dprop}(\omega)||$, the sum of error $E_{sum} = \sum_{k=1}^{512} (E_m(\omega_k))^2$, and total phase error $T_{phase} = \sum_{k=1}^{512} |\angle G_{dprop}(\omega_k)|$.

The program is executed for several times to decide the optimal value of the weight, w (= 0.8). Due to the absence of any golden rule to find the optimal value of w, initially, the proposed Riesz FODD design problem is initiated without assigning the weight (w) term in the cost function as defined in (10). Afterwards, a more significant value of w is put to minimise T_{phase} and E_{max}, which are regarded as the principal objectives of the present study. An exhaustive trial runs of the algorithm is performed for several times with different values of w until almost zero-phase response and near-ideal magnitude characteristics are obtained.

The performances among the designed Riesz FODDs along with those of other approaches are compared by employing maximum absolute magnitude error ($MAME$) = $\max[||G_i(\omega)| - |G_{dprop}(\omega)||]$, total error = $sum[||G_i(\omega)| - |G_{dprop}(\omega)||]$, and maximum phase error (MPE) = $\max[|\angle G_{dprop}(\omega)|]$ metrics.

IV. EMPLOYED EVOLUTIONARY ALGORITHMS

Algorithms based on natural evolution like MRFO [25], ABC [28], and FPA [29] along with classical optimisation methods such as LS [26] and CVXO [27] are employed to realise the proposed Riesz FODDs. In literature, the LS, CVXO, ABC, and FPA are frequently used to optimise several real-world problems [30]–[32]. The explanations of LS, CVXO, ABC, and FPA are, therefore, not included in this

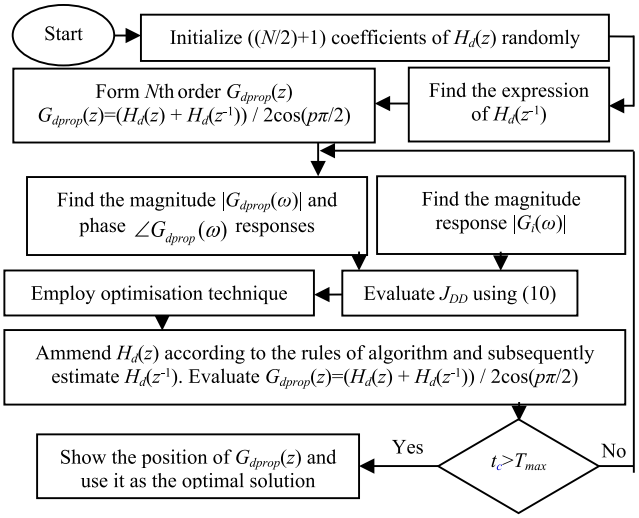

FIGURE 1. The proposed Riesz FODD design scheme.

article because of the space constraint. Interested readers may review these algorithms mentioned in [30]–[32]. However, the next sub-section includes the step-wise procedure of the MRFO algorithm for developing the proposed Riesz FODD.

A. MANTA-RAY FORAGING OPTIMIZATION (MRFO)

MRFO algorithm mathematically models three different manta ray's foraging mechanisms, such as cyclone foraging, somersault foraging, and chain foraging for optimisation purposes as described in the below steps.

Step 1. By employing (11) disperse n_p manta rays (population) within the D dimensional quest landscape.

$$x_j^i(t_c) = lb + rand \times (ub - lb), \quad i = 1, 2, \ldots, n_p; \quad j = 1, 2, \ldots, D. \tag{11}$$

where $x_j^i(t_c)$ denotes i^{th} manta ray position in the j^{th} dimension. ub and lb denote upper and lower ranges of the questing environment of the Riesz FODD design problem. $rand \in [0, 1]$ represents the random number.

Step 2. Use (10) to quantify the fitness J_{DD} of each manta ray and get the best solution found x_{best} so far.

Step 3. For each manta ray x^i, for $i = 1, 2, \ldots, n_p$, execute *Step* 4 to *Step* 7.

Step 4. If $rand < 0.5$, then jump to *Step* 5 to perform cyclone foraging, else jump to *Step* 6 to perform chain foraging.

Step 5. If $(t_c/T_{max}) < rand$, update the location of manta rays using (12) and (13), else, amend the position of manta rays using (14). It is noteworthy that (13) is used to perform an extensive local search, whereas, (14) promotes an exhaustive global search mechanism of the MRFO algorithm.

$$x_{rand} = lb + rand \times (ub - lb) \tag{12}$$

$$x_j^i(t_c+1) = \begin{Bmatrix} x_{rand} + r \cdot \left(x_{rand} - x_j^i(t_c)\right) + \cdots \\ \beta \cdot \left(x_{rand} - x_j^i(t_c)\right) \quad for\ i = 1 \\ x_{rand} + r \cdot \left(x_j^{i-1}(t_c) - x_j^i(t_c)\right) + \cdots \\ \beta \cdot \left(x_{rand} - x_j^i(t_c)\right) \quad for\ i = 2, \ldots, n_p \end{Bmatrix} \tag{13}$$

$$x_j^i(t_c+1) = \begin{Bmatrix} x_{best} + r \cdot \left(x_{best} - x_j^i(t_c)\right) + \cdots \\ \beta \cdot \left(x_{best} - x_j^i(t_c)\right) \quad for\ i = 1 \\ x_{best} + r \cdot \left(x_j^{i-1}(t_c) - x_j^i(t_c)\right) + \cdots \\ \beta \cdot \left(x_{best} - x_j^i(t_c)\right) \quad for\ i = 2, \cdots, n_p \end{Bmatrix} \tag{14}$$

where T_{max} and t_c denote the maximum and the current number of iteration, respectively. x_{rand} represents the randomly generated position. $r \in [0, 1]$ represents the random number. β is the weight coefficient defined in (15).

$$\beta = 2 \cdot \exp(r_1(T_{\max} - t_c + 1)/T_{\max}) \cdot \sin(2\pi\, r_1) \tag{15}$$

where $r_1 \in [0, 1]$ represents the random number.

Step 6. Adjust the manta rays position using (16).

$$x_j^i(t_c+1) = \begin{Bmatrix} x_j^i(t_c) + r \cdot \left(x_{best} - x_j^i(t_c)\right) + \cdots \\ \alpha \cdot \left(x_{best} - x_j^i(t_c)\right) \quad for\ i = 1 \\ x_j^i(t_c) + r \cdot \left(x_j^{i-1}(t_c) - x_j^i(t_c)\right) + \cdots \\ \alpha \cdot \left(x_{best} - x_j^i(t_c)\right) \quad for\ i = 2, \cdots, n_p \end{Bmatrix} \tag{16}$$

where the weight coefficient a is defined in (17)

$$\alpha = 2 \cdot r \cdot \sqrt{|\log(r)|} \tag{17}$$

Step 7. Use (10) to quantify the fitness J_{DD} of each manta ray and adjust x_{best}.

Step 8. For each manta ray x^i, for $i = 1, 2, \ldots, n_p$, execute *Step* 9 to *Step* 10 to perform the somersault foraging.

Step 9. Adjust the manta rays position using (18).

$$x_j^i(t_c+1) = x_j^i(t_c) + S \cdot \left(r_2 \cdot x_{best} - r_3 . x_j^i(t_c)\right) \tag{18}$$

where S $(= 2)$ is the somersault factor and $(r_2, r_3) \in [0, 1]$ are the random numbers.

Step 10. Employ (10) to measure the fitness J_{DD} of each manta ray and amend x_{best}.

Step 11. Execute *Step* 3 to *Step* 10 until T_{max} is reached.

Step 12. After completing T_{max}, return the x_{best} position and proclaim it as the optimal solution of the Riesz FODD.

Due to space limitation, the pseudo-code of the evolutionary MRFO algorithm to evaluate the optimal solution for the Riesz FODD type optimisation problem is given in supplementary file as Algorithm 1.

V. PROPOSED R-PEAK DETECTION METHODOLOGY

The proposed Riesz FODD based QRS complex detector is portrayed in Fig. 2, where the proposed Riesz FODD of order $p = 0.5$ substitutes the conventional FODD in the QRS related feature signal generation stage of a recently proposed

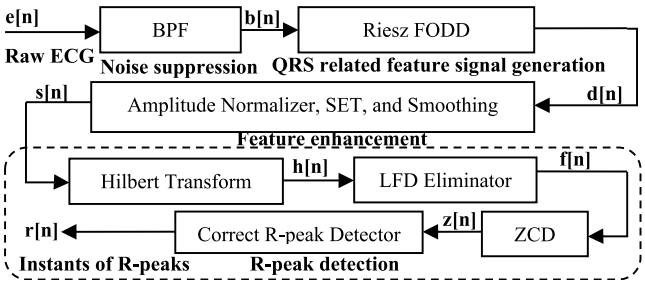

FIGURE 2. QRS complex detection methodology.

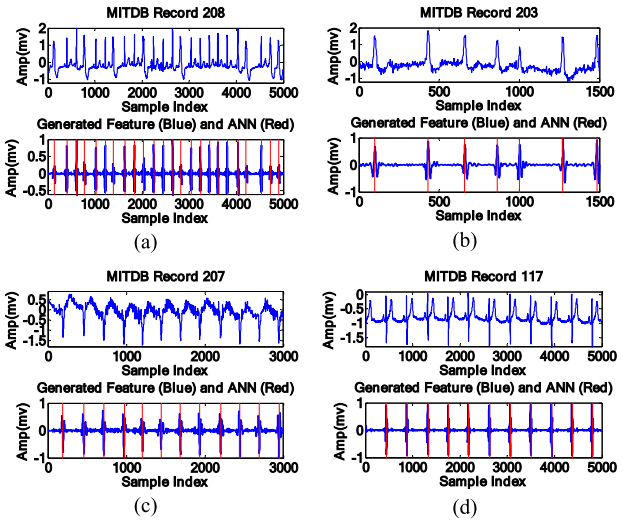

FIGURE 3. Illustration of generated feature signal, d[n] for numerous abnormal ECG excerpts extracted from MITDB: (a) ECG with premature ventricular contraction beats, (b) ECG with muscle noise, (c) ECG with inverted QRS complex, and (d) ECG with high amplitude T-wave.

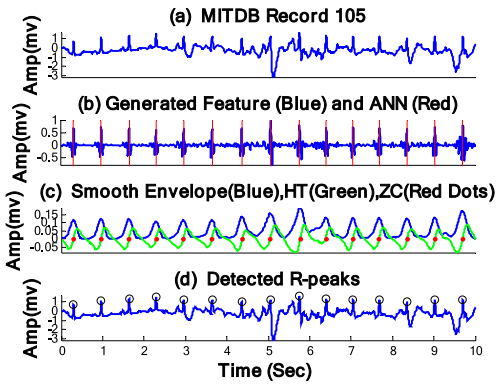

FIGURE 4. Proposed QRS detection methodology: (a) ECG record 105 of MITDB, (b) output of Riesz fractional order digital differentiator (FODD), annotation (ANN), (c) smooth envelope, the output of Hilbert Transform (HT), zero crossings (ZCs), and (d) detected R-peaks (black circle).

ECG QRS detector [19] to augment the correctness of the QRS detection. The proposed Riesz FODD possesses a zero-phase property which assists in preserving the features of the differentiated ECG precisely at the same time instant where they occur in the unfiltered signal. Additionally, the optimal MR of the proposed Riesz FODD helps to obtain highly accurate differentiated ECG.

The collaboration of two indigenous features of the proposed Riesz FODD, such as optimal magnitude and zero-phase response is instrumental in the QRS complex detection application and assists in locating the R-peaks with improved precision in the ECG signal. These two unique behaviours of the proposed Riesz FODD are explored in the following subsections through several real ECG signals.

The input raw ECG signal ($e[n]$) is sequentially processed through four independent signal processing blocks, such as (i) noise suppression, (ii) QRS related feature signal generation, (iii) feature enhancement, and (iv) R-peak detection module to identify the R-peak location, $r[n]$ precisely. The working of all the four independent blocks is studied in the following sub-sections. ECG with a signal duration of 10 seconds is considered for the majority of ECG based applications, such as heart rate variability (HRV) analysis, ECG beat classification, ECG compression, etc. Thus, each ECG signal in this study is split into several sub-blocks of 10 seconds duration. Next, R-peaks are identified by processing each block independently. This operation facilitates the proposed Riesz FODD based QRS complex detector for online identification of R-peaks. Additionally, the proposed QRS detector processes each ECG sample in only 3.7 µs. Thus, to process a 10 s ECG signal sampled at 360 Hz, the proposed algorithm will take only 0.013 s. Hence, the proposed QRS detector can be easily realised in real-time in block-by-block processing mode.

A. NOISE SUPPRESSION FOLLOWED BY QRS RELATED FEATURE SIGNAL GENERATION STAGES

Numerous artefacts and noise sources frequently corrupt the recorded ECG signals. Notably, the existence of these noises and artefacts in the ECG register increases the false heartbeat count. The majority of the QRS complex energy resides within a narrow frequency range from 5-22 Hz [19]. So, firstly, the undesired ECG regions are separated by employing a (5-22 Hz) Chebyshev type-1 bandpass filter (BPF) of the third order. Next, the MRFO based Riesz FODD of fractional order $p = 1/2$ has been employed to generate QRS related feature signal by convolving the bandpass filtered ECG with the proposed Riesz FODD coefficients. Moreover, this convolution operation again minimises the effect of the T/P-peaks. Figs. 3(a)–(d) and Figs. 4(a)–(b) show the generated feature signals, $d[n]$ for numerous abnormal ECG excerpts. From the differentiation outcomes, as portrayed in Figs. 3(a)–(d) and Fig. 4(b), it is noticed that due to its almost zero-phase and near-ideal magnitude characteristic, the proposed Riesz FODD emphasises the QRS region precisely at the same time instant where they occur in the input ECG signal by suppressing various noise and artefacts. As a result, both the differentiated output and the database annotation (ANN) coincide with

each other (refer to the second subplots of Figs. 3(a)–(d) and Fig. 4(b)).

B. FEATURE ENHANCEMENT STAGE

In the feature enhancement stage, the zero-phase differentiated ECG signal, $d[n]$ is further processed by three cascaded signal processing stages such as

(i) Amplitude normaliser ($a[n] = d[n]/\max_{n=1}^{K}(|d[n]|)$, where K denotes the total number of ECG signal samples),

(ii) Shannon energy transformer (SET) ($e_s[n] = -((a[n])^2.\log\ (a[n])^2)$), and

(iii) Moving average (MA) type smoothing filter ($s[n] = (1/M)\sum_{m=0}^{M-1} e_s[n-(M-1-m)]$, where M (= 55) is the length of the MA filter) to generate smooth envelope (refer to the blue line in Fig. 4(c)) corresponding to the QRS complex region.

C. R-PEAK DETECTION LOGIC

The local maximum in each smooth envelope provides the approximate R-peak location in the ECG signal. The local maximum is identified by utilising the odd symmetry property of the HT (refer to Fig. 4(c)). In Fig. 4(c), the smooth envelope is depicted in blue, and its corresponding HT is depicted in green. From Fig. 4(c), it is evident that due to the anti-symmetric nature of the HT, the HT sequence crosses the zero axis during every inflexion point in the smooth envelope. The location of zero crossings (ZCs) (red dots in Fig. 4(c)) is detected by determining the sign of input signal at the time instants t_n and t_{n+1}. The experiment shows a minimal difference between the location of ZCs and true R-peaks. Consequently, the true occurrences of the R-peaks are identified by calculating the absolute maximum amplitude in the raw ECG signal within ±25 samples around each ZC location. The detected R-peaks are marked in a black circle in Fig. 4(d).

Furthermore, the experiment shows that, in some instants, the HT sequence drifts from the reference line, called low-frequency drift (LFD). In general, due to the shifting of the baseline and due to the sudden variation of peak amplitudes, the LFD appears. The LFD problem increases false heartbeat detection (FHBD). To solve this problem, a rectangular window type MA filter with filter length $K = 400$ is used. For this, firstly, the HT sequence is filtered by the MA filter, and then its output is subtracted from the HT sequence. Finally, LFD free ECG is further processed in the zero-crossing detector (ZCD) and correct the R-peak detector stages for identifying the exact R-peak position.

VI. RESULTS AND DISCUSSION

A. SIMULATION RESULTS OF THE PROPOSED RIESZ FODD

To design the FIR-type 22nd order Riesz FODDs using LS, CVXO, ABC (limit value: 100), FPA (scaling factor γ: 0.12; step size *s:* 1.25; lévy distribution factor λ: 1.50; switch probability *p:* 0.75), and MRFO (somersault factor *S:* 2), extensive MATLAB simulations have been carried out. Common control variables such as n_p (= 50), maximum number of function evaluations FE_{max} (=$10^4 \times D$), D (= 22), and $[l_b \quad u_b]$ (= [−2 2]) for all EAs are kept uniform. The relationship between FE_{max} and T_{max} is given as $FE_{max} = e_t \times n_p \times T_{max}$. Here e_t represents the number of times the fitness function is calculated in one iteration. Due to space crunch, the optimal coefficients of the FIR-type Riesz FODDs of fractional order $p = 1/2$ resulted from the employed EAs are given in Table A in the supplementary file. However, the performance metrics of the FIR-type Riesz FODDs are presented in Table 1. Comparison summary of the percentage improvement obtained by the employed EAs for the realisation of Riesz FODDs in terms of MAME and MPE is presented in Table 2. The MRFO algorithm results in improved design performances compared to the LS, CVXO, ABC, and FPA counterpart for the proposed Riesz FODD design.

TABLE 1. Performance of the 22nd order Riesz FODDs designed using LS, CVXO, ABC, FPA, and MRFO for $p = 1/2$.

Algorithm	MAME	MAME (dB)	Total error	MPE (degree)
LS	0.5100	-5.8479	41.5188	4.2305E-014
CVXO	0.4772	-6.4251	32.9665	4.0516E-014
ABC	0.4268	-7.3961	29.22	3.8778E-014
FPA	0.3471	-9.1900	29.49	3.7160E-014
MRFO	**0.2298**	**-12.7742**	**4.79**	**2.9757E-014**

The zero-phase characteristic of the proposed Riesz FODDs for $p = 1/2$ is justified through several FR comparison plots: (i) phase (in degree) plot (portrayed in Fig. 5(a)), (ii) absolute phase error (in degree) plot (portrayed in Fig. 5(b)), (iii) phase delay (in samples) plot (portrayed in Fig. 5(c)), and group delay (in samples) plot (portrayed in Fig. 5(d)). Figs. 5(e)–(f) present the MR and absolute magnitude error (AME) (in dB) comparison plots, respectively, of the designed Riesz FODDs for $p = 1/2$ along with the ideal Riesz FOD magnitude characteristic. In Fig. 5(e), the MR of the designed MRFO-based Riesz FODD accurately approximates the ideal Riesz FOD response for the normalised frequency ranges of −1 to −0.01 and 0.01 to 1.0.

For QRS detection system, initially, the raw ECG is passed through a 5-22 Hz BPF. The sampling frequency (F_s) of TWADB, MITDB, NSTDB, EDB, SVDB, and AFTDB are 500 Hz, 360 Hz, 360 Hz, 250 Hz, 128 Hz, and 128 Hz, respectively. In normalised frequency, with *Fs* of 128 Hz, 250 Hz, 360 Hz, and 500 Hz, the range of 5–22 Hz of the BPF is converted to the range of 0.078–0.344, 0.04–0.176, 0.027–0.122, and 0.02–0.088, respectively [14]. As the MR of the proposed MRFO-based Riesz FODD accurately approximates the ideal Riesz FOD response for the normalised frequency range of 0.01–1.0, the proposed Riesz FODD generates highly accurate differentiated output and assists the QRS identification task.

1) ROBUSTNESS ANALYSIS

The statistical analysis is performed by running the employed EAs for 50 times to estimate several statistical metrics as

TABLE 2. Comparison Summary of the Percentage Improvement in Terms of MPE and MAME for the 22nd order Riesz FODD.

MPE (degree) (×E-014)					Percentage improvement in terms of MPE			
LS	CVXO	ABC	FPA	MRFO	MRFO and LS	MRFO and CVXO	MRFO and ABC	MRFO and FPA
4.2305	4.0516	3.8778	3.7160	2.9757	30	26	23	20
MAME					**Percentage improvement in terms of MAME**			
LS	CVXO	ABC	FPA	MRFO	MRFO and LS	MRFO and CVXO	MRFO and ABC	MRFO and FPA
0.5100	0.4772	0.4268	0.3471	0.2298	55	52	46	34

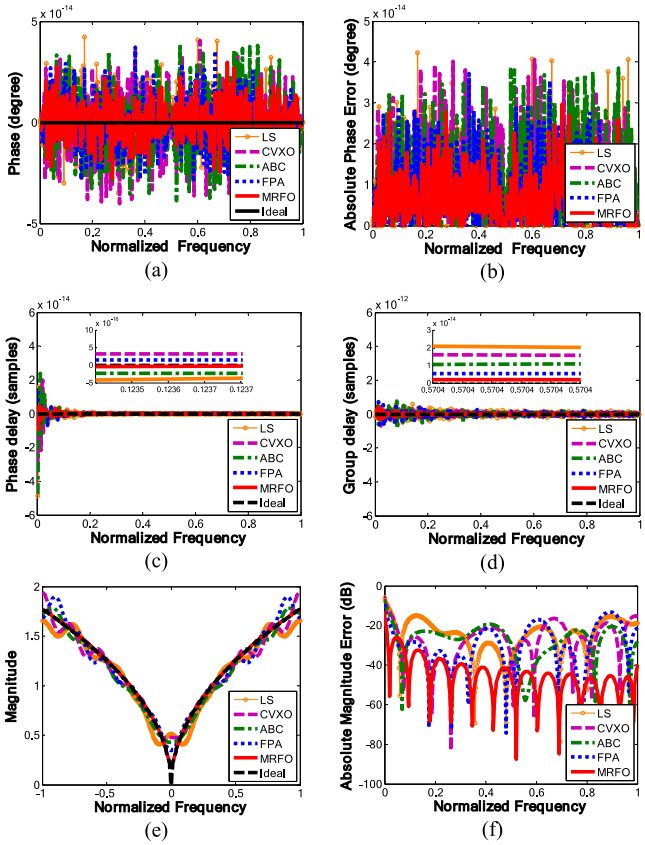

FIGURE 5. Frequency response plots of the LS, CVXO, ABC, FPA, and the MRFO-based Riesz fractional order digital differentiators for p=1/2: (a) phase response, (b) absolute phase error, (c) phase delay, (d) group delay, (e) magnitude response, and (f) absolute magnitude error.

TABLE 3. Statistical Data of Riesz FODDs.

Statistical Data	Best	Worst	Average	Median	SD
Algorithm			**MAME (dB)**		
LS	-5.8479	-1.7245	-3.4726	-3.4586	1.4834
CVXO	-6.4251	-2.1549	-4.1362	-4.5698	1.5000
ABC	-7.3961	-3.1579	-5.4482	-5.3935	1.4502
FPA	-9.1900	-4.3015	-7.0205	-7.2000	1.9027
MRFO	-12.774	-8.1295	-12.111	-12.380	0.9047
Algorithm			**Computational time in second**		
LS	40.8564	41.2158	40.9845	41.0214	0.0975
CVXO	48.1297	48.8954	48.4518	48.4429	0.0917
ABC	69.4510	69.8103	69.5795	69.5784	0.0889
FPA	72.2519	72.8712	72.4105	72.3909	0.0912
MRFO	64.3860	64.6560	64.4555	64.4520	0.0703
Algorithm			**Number of function evaluations needed**		
LS	11550	23300	21600	21700	257
CVXO	12450	22600	21100	21250	253
ABC	19700	20950	20050	20150	243
FPA	19000	20700	19850	19750	245
MRFO	20200	21600	20700	20600	212

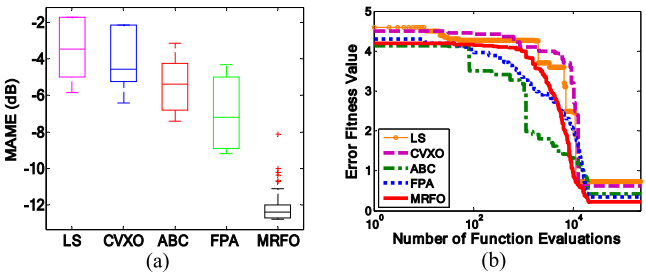

FIGURE 6. The response of the proposed Riesz FODDs: (a) box plot showing a slight difference in the MAME metric those are obtained in individual runs of the algorithm, and (b) convergence profile.

shown in Table 3 and Fig. 6(a) in terms of the MAME metric and box and whisker plot, respectively. Note that MRFO supersedes LS, CVXO, ABC, and FPA in the average values of the MAME metrics. This ensures steady supremacy of MRFO over LS, CVXO, ABC, and FPA for the proposed Riesz FODD design problem. Additionally, the SD of the MRFO-based Riesz FODD design is the lowest among all the Riesz FODD designs, which confirms the robust behaviour of the proposed method for the Riesz FODD design problem.

2) ANALYSIS OF COMPUTATIONAL EFFICIENCY

The employed algorithm which evaluates the fitness function maximum number of times in one second is considered as the fastest algorithm having the lowest computational complexity in solving the Riesz FODD design problem. The best so far convergence of the error fitness values resulted from the employed EAs are portrayed in Fig. 6(b). To establish the robust behaviour of the adopted algorithms in terms of convergence profile and computational time, 50 independent trial runs are performed. Various statistical parameters are shown in Table 3. The outcomes demonstrate that compared to LS, CVXO, ABC, and FPA, the MRFO evaluates the fitness function for the maximum number of 313 (= 20200/64.3860) times in one second and is the fastest among all the employed algorithms to attain the lowest error cost value. Whereas, the LS, CVXO, ABC, and FPA evaluate the fitness function only for 282 (= 11550/40.8564), 258 (= 12450/48.1297), 283 (= 19700/69.451), and 262 (= 19000/72.2519) times, respectively, in one second.

TABLE 4. Wilcoxon rank-sum test.

N	Advanced algorithm	n_1	n_2	Wilcoxon rank-sum test: Critical value 0.05	Critical value 0.01	Order of the Riesz FODD (p=1/2) W_1	W_2	Accept/reject (CL)
22	LS	7	11	44	38	28	143	Reject (99%)
		10	12	85	76	55	198	Reject (99%)
	CVXO	7	11	44	38	37	134	Reject (99%)
		10	12	85	76	64	189	Reject (99%)
	ABC	7	11	44	38	37	134	Reject (99%)
		10	12	85	76	56	197	Reject (99%)
	FPA	7	11	44	38	40	131	Reject (95%)
		10	12	85	76	68	185	Reject (99%)

3) CONSISTENCY ANALYSIS

The comparison of performance consistency among the MRFO technique and the advanced LS, CVXO, FPA, and ABC for the Riesz FODD design problem is demonstrated by using Wilcoxon rank-sum test [33] over the datasets of the applied algorithms based on pairwise unions of LS-MRFO, CVXO-MRFO, ABC-MRFO, and FPA-MRFO.

To execute these tests, the null hypothesis (H_0) is believed to be as no significant difference in terms of MAME metric for the realised Riesz FODDs exists between the two datasets resulted from the advanced algorithm and the MRFO algorithm. n_1 and n_2 represent the swarm size and W_1 and W_2 represent the sum of ranks of advanced and the proposed algorithm, respectively. The rejection or acceptance of the null hypothesis is decided by comparing W_1 and W_2 values with the critical values related to each significance level, as stated in [33]. The outcomes of the hypothesis experiment, as presented in Table 4, confirm that the MRFO discards the null hypothesis with a reasonably high value of confidence level. Thus, the MRFO algorithm consistently accomplishes the lowest values of MAME metric compared to LS, CVXO, ABC, and FPA based Riesz FODD designs.

4) COMPARATIVE STUDY

In Table 5 and Fig. 7, the performance parameters of the proposed LS, CVXO, ABC, FPA, and MRFO based FIR-type Riesz FODDs of fractional order $p = 0.5$ are compared with the FD based IIR-type Riesz FODD [21], [24], Tustin's method based IIR-type Riesz FODD [21], and DCT based FIR-type Riesz FODD [21] to exhibit the design efficiency of the proposed method. From Fig. 7, it can be seen that the Riesz FODs designed by the FD (for $p = 0.5$ and 0.6) and the Tustin's method (for $p = 0.5$) approximate the ideal Riesz FOD counterparts only at the low-frequency band around $\omega = 0$. Additionally, the FD and Tustin's method based Riesz FODs is IIR filters with an infinite duration. In [21] and [24], the FD and Tustin's method based Riesz FODs are realised by truncating the infinite duration Riesz FODs to lower-order IIR filter by adopting Prony's method [21]. Thus, due to truncation, the approximation error is further increased around $\omega = 0$ [21]. Moreover, from Table 5 and Fig. 7, it is clear that compared to the best Riesz FODD model (MAME = 0.2298) designed by MRFO algorithm, the DCT

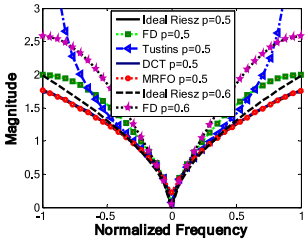

FIGURE 7. Comparative analysis among the proposed and the reported Riesz FODDs in terms of magnitude responses.

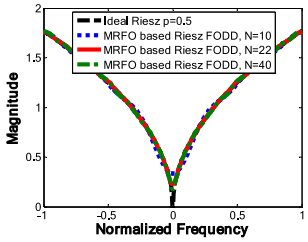

FIGURE 8. Magnitude responses of N = 10th, 22nd, and 40th order MRFO-based Riesz FODDs.

based 99th order FIR-type Riesz FODD model [21] provides the lowest reported MAME value of 0.1984. However, the proposed Riesz FODD provides a low complex structure and low data latency due to the lower order design ($N = 22$) compared to the higher-order ($N = 99$) DCT based Riesz FODD model which needs more hardware resource and higher data latency.

Likewise, the same design procedure, as discussed above, is followed to design both lower-order ($N = 10$) and higher-order ($N = 40$) Riesz FODD models which provide lower and higher design accuracy, respectively, compared to the proposed 22nd order Riesz FODD model (refer to Table 6 and Fig. 8). However, for the proposed Riesz FODD based QRS identification application, the Riesz FODD of order $N = 22$ is the most suitable choice compared to both lower and higher-order Riesz FODD models in terms of design accuracy and computational complexity. The lower order design ($N = 10$) is hardware efficient, but, a poor rational approximation to its corresponding ideal counterpart is achieved in this case. Due to this, more number of false beats are identified (refer to Table 6) when $N = 10$th order Riesz FODD based QRS detector (refer to Fig. 2) is tested against MITDB ECG signals. Alternatively, although the higher-order models achieve improved rational approximation to their corresponding ideal counterpart compared to the lower order designs; however, in terms of $FHBD(= FP + FN)$, the performance of $N = 40$th order Riesz FODD based QRS detector is not significantly improved compared to $N = 22$nd order Riesz FODD based QRS detector when tested against MITDB ECG signals (refer to Table 6). Conversely, the physical design of the higher-order models needs more hardware resources and thereby, yields more data latency.

TABLE 5. Comparative study between the proposed and the reported Riesz FODDs of order p=1/2.

Literature	Method	p	MAME	MAME (dB)	Total error
Tseng *et al.* [21]	FD (Fig. 1)	0.5	0.3528	-9.04	235.2
	Tustin's (Fig. 3)	0.5	1.8073 E+008	165.14	3.6146 E+008
	DCT (Fig. 4)	0.5	0.1984	-14.04	4.04
Kaur *et al.* [24]	FD	0.6	0.7207	-2.84	119.0
Present work	LS	0.5	0.5100	-5.8479	41.51
	CVXO	0.5	0.4772	-6.4251	32.96
	ABC	0.5	0.4268	-7.39	29.22
	FPA	0.5	0.3471	-9.19	29.49
	MRFO	0.5	0.2298	-12.77	4.79

() signifies the figure number in the corresponding reference where the Riesz differentiator has been reported, [] signifies the reference number

TABLE 6. MAME, MPE, and FHBD performance metrics.

N	MAME (dB)	MPE (degree)	FHBD of MITDB
10	-9.5110	2.0301E-014	196
22	-12.7742	2.9757E-014	110
40	-15.0928	4.2854E-014	107

5) OPTIMAL SELECTION OF FRACTIONAL ORDER (p) OF RIESZ FODD

The fractional order (p) of the FODD is application-specific. Thus, it is necessary to select the optimal fractional order (p_{opt}) of the Riesz FODD for ECG QRS detection application. For this, firstly, the proposed Riesz FODD design approach is used to realise several Riesz FODDs for different values of p. Fig. 9 shows the MR comparison plots of the Riesz FODDs for different values of p, and its corresponding performance metrics are depicted in Table 7. Secondly, the designed Riesz FODDs for several values of p are individually employed to realise QRS related feature signal generation stage of the proposed QRS detector (refer to Fig. 2). Finally, the efficacy of the designed QRS detector is verified by using the MITDB, EDB, NSTDB, SVDB, TWADB, and AFTDB ECG signals. The performance corresponding to MITDB in terms of the total number of *FHBD* metric is presented in Table 7. From Table 7, it is clear that the lowest *FHBD* is found for p=0.5. Additionally, for EDB, NSTDB, SVDB, TWADB, and AFTDB, the lowest *FHBD* has also been resulted for p=0.5 (refer to Figs. 10(a)–(b)). Thus, from Table 7 and Figs. 10(a)–(b), it is clear that the optimal value (p_{opt}) of the Riesz FODD for ECG QRS detection application is 0.5.

B. SIMULATION RESULTS OF THE PROPOSED MRFO-RIESZ FODD BASED QRS DETECTOR

ECG signals of MITDB, EDB, NSTDB, SVDB, AFTDB, and TWADB are employed to validate the Riesz FODD-based QRS detector. All of these ECG datasets are publicly available at PhysioNet [34]. Due to space constraint, the features of each database are depicted in Table B in the supplementary file. The performance measuring indices, such as $DER = (FP + FN)/(\text{Total number of QRS complexes})$, $PP = TP/(TP + FP)$, and $Se = TP/(TP + FN)$ are employed for validating the accuracy of the R-peak detector. Additionally, the preciseness of the designed QRS detector is examined by evaluating the meantime error *MTE* (ms) $= (\sum_{i=0}^{TP} |QRS_i - QRS_{ANN}|)/TP$ between the time of occurrence of the identified ECG beat (QRS_i) and database annotation (QRS_{ANN}). Here, *TP*, *FN*, and *FP* stand for the total number of truly identified, unidentified, and falsely identified heartbeats, respectively.

TABLE 7. MAME, MPE, and FHBD performance metrics.

p	MAME (dB)	MPE (degree)	FHBD of MITDB
0.1	-2.6280	3.6655e-014	190
0.2	-5.1937	4.6403e-014	150
0.3	-9.6573	3.1189e-014	146
0.4	-10.2480	3.4678e-014	140
0.5	**-12.7742**	**2.9757E-014**	**110**
0.6	-15.5987	4.0617e-014	153
0.7	-18.0164	4.1220e-014	160
0.8	-20.6304	3.6465e-014	165
0.9	-23.4701	3.6161e-014	167
1.0	-29.7691	4.9889e-014	171

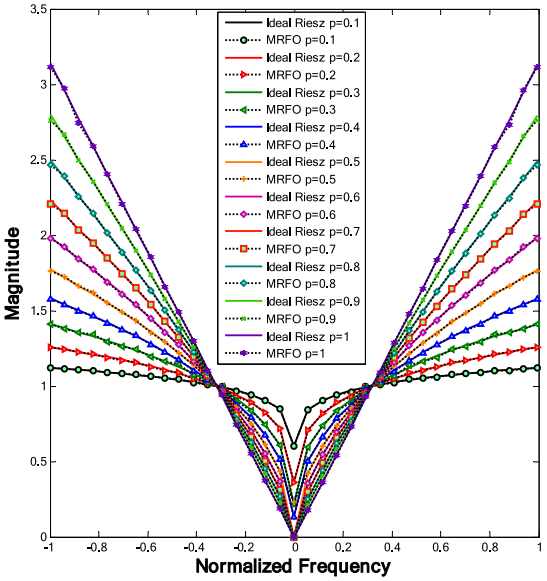

FIGURE 9. Magnitude responses of the proposed Riesz FODDs.

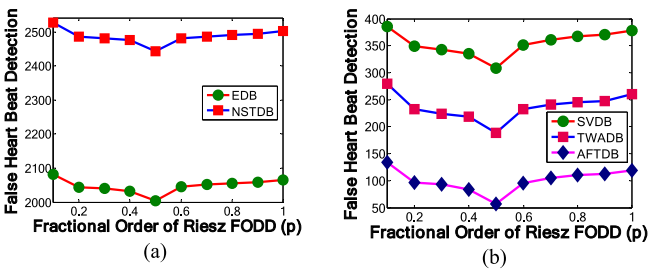

FIGURE 10. Obtained QRS identification results (in terms of false heartbeat detection) for different fractional order (p) of the Riesz FODD against (a) EDB and NSTDB and (b) SVDB, TWADB, and AFTDB.

TABLE 8. Performance comparison with the previous studies validated against PhysioNet ECG datasets.

Database	Publication	Total beats	*TP beats*	*FP beats*	*FN beats*	*Se* (%)	*PP* (%)	*DER* (%)	*POI_FP*	*POI_FN*	*MTE* (ms)
MITDB	Hou *et al*. [5]	110008	109254	610	748	99.3	99.4	1.2	89	94	N/R
	Tang *et al*. [6]	109966	109055	494	911	99.1	99.5	0.2	87	95	2.309
	Yazdani *et al.* [7]	110070	109967	134	103	99.9	99.8	0.2	51	57	N/R
	Choi *et al*. [12]	109118	108742	218	376	99.6	99.8	0.5	69	88	7.75
	Benitez *et al*. [13]#	45856	45828	30	28	99.9	99.9	0.1	-120	-57	3.03
	Yakut *et al*. [15]	109494	109310	182	184	99.8	99.8	0.2	64	76	N/R
	Khamis *et al.* [16]@	109494	N/R	N/R	N/R	99.2	99.0	*	*	*	3.81
	Khamis *et al.* [16]$	109494	N/R	N/R	N/R	99.6	99.4	*	*	*	11.18
	Khamis *et al.* [16]%	109494	N/R	N/R	N/R	99.7	99.8	*	*	*	6.04
	Nayak *et al*. [19]	109494	109442	70	52	99.9	99.9	0.1	6	15	2.284
	Kaur *et al.* [24]	109498	109448	54	55	99.9	99.9	0.1	-22	20	N/R
	Proposed Method	**109494**	**109450**	**66**	**44**	**99.9**	**99.9**	**0.1**			**0.851**
EDB	Martinez *et al*. [2]	787103	784059	4077	3044	99.6	99.4	0.9	75	68	N/R
	Dohare *et al*. [4]	790559	774180	2190	3679	99.5	99.7	0.7	53	74	N/R
	Sharma et al. [8] #	92403	92205	288	196	99.8	99.6	0.5	-260	-393	N/R
	Pandit *et al*. [9]	790495	788746	2208	1749	99.7	99.7	0.5	53	45	N/R
	Yakut *et al*. [15]	790565	787514	1371	3051	99.6	99.8	0.5	24	68	N/R
	Nayak *et al*. [19]	790560	789536	1117	1024	99.8	99.8	0.2	7	6	2.341
	Proposed method	**790560**	**789593**	**1037**	**967**	**99.8**	**99.8**	**0.2**			**0.91**
NSTDB	Khamis *et al*. [16]@	25590	N/R	N/R	N/R	93.1	81.8	*	*	*	5.83
	Khamis *et al*. [16]$	25590	N/R	N/R	N/R	91.6	86.4	*	*	*	14.17
	Khamis *et al*. [16]%	25590	N/R	N/R	N/R	93.1	87.1	*	*	*	11.58
	Dohare *et al*. [4]	25590	22759	2806	3049	88.1	89.0	22.8	56	60	N/R
	Yakut *et al*. [15]	25590	23957	1389	1633	93.6	94.5	11.8	11	26	N/R
	Proposed method	**25590**	**24381**	**1235**	**1209**	**95.2**	**95.1**	**9.5**			**1.736**
SVDB	Burguera [10]	184744	N/R	N/R	N/R	96.6	99.1	*	*	*	N/R
	Nayak *et al*. [19]	184582	184421	179	161	99.9	99.9	0.2	20	15	2.292
	Proposed method	**184582**	**184446**	**142**	**136**	**99.9**	**99.9**	**0.1**			**0.857**
AFTDB	Elgendi [10]	7618	N/R	N/R	N/R	99.7	99.7	*	*	*	N/R
	Burguera [11]	7618	N/R	N/R	N/R	88.6	96.9	*	*	*	N/R
	Proposed method	**7592**	**7577**	**11**	**15**	**99.8**	**99.8**	**0.3**			**0.945**
TWADB	Burguera [12]	**19003**	**N/R**	**N/R**	**N/R**	**91.9**	**99.5**	*	*	*	**N/R**
	Nayak *et al*. [19]	**18993**	**18884**	**142**	**109**	**99.43**	**99.25**	**1.3**	**28**	**20**	**2.389**
	Proposed method	**18993**	**18906**	**102**	**87**	**99.5**	**99.5**	**0.9**			**0.97**

'*': Metric could not be evaluated because of insufficient data; 'N/R': Not reported; '#': QRS detector is validated against a comparatively lesser number of beats; '@': Pan-Tompkins algorithm evaluated in [16]; '$': Gutierrez-Rivas algorithm evaluated in [16]; '%': UNSW algorithm validated in [16].

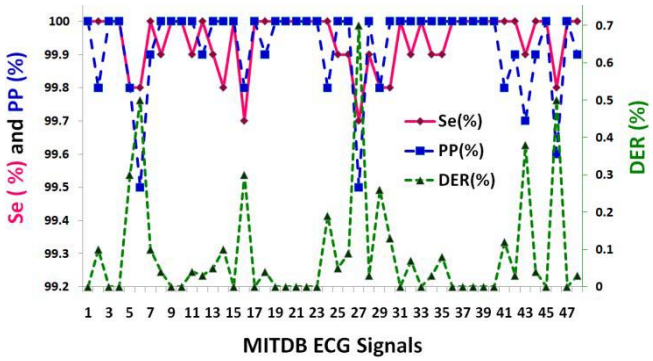

FIGURE 11. Performance of the proposed QRS detector in terms of *Se*, *PP*, and *DER* validated against all 48 MITDB ECG signals.

1) PERFORMANCE OF THE QRS DETECTOR AGAINST MITDB

In Fig. 11, the record-wise performance of the proposed QRS detector against MITDB ECG signals in terms of *Se*, *PP*, and *DER* is portrayed. Results presented in Fig. 11 confirm that the proposed R-peak detector performs satisfactorily and detects the heartbeats most accurately. Besides the presence of artefacts and noise in the MITDB, the morphology of the ECG records is very complicated and varies from one ECG record to another. The proposed QRS complex detector performs well in all the abnormal conditions. The performance of the proposed R-peak detection methodology for some critical ECG fragments extracted from several records is illustrated in Figs. 12(a)–(d) as an example. From Figs. 12(a)–(d), it is evident that all the R-peaks are identified successfully with the proposed technique. It is because of the robust feature inducing ability of the proposed Riesz FODD-based feature signal generating stage.

2) PERFORMANCE COMPARISON

Table 8 shows the summary of the performance comparison among the existing high performance and the proposed QRS complex detection approaches which are validated against the first channel records of MITDB, EDB, NSTDB, SVDB,

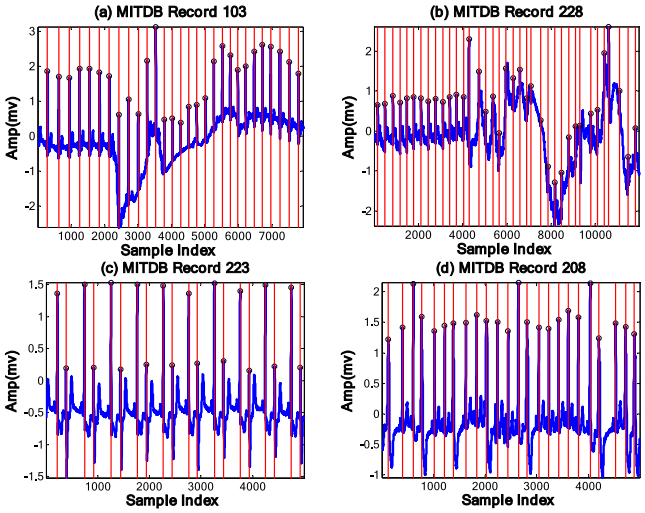

FIGURE 12. Illustration of R-peak identification against the MITDB (in each figure, the extracted ECG fragment is illustrated in blue, the black circle shows the identified R-peaks, and the MITDB annotations are illustrated in red standing lines): (a) Record-103: ECG segment with severe baseline shifting, (b) Record-228: ECG segment with tiny QRS waves, (c) Record-223: ECG segment with sudden peak amplitude fluctuation, (d) Record-208: ECG segment with premature ventricular contraction beats.

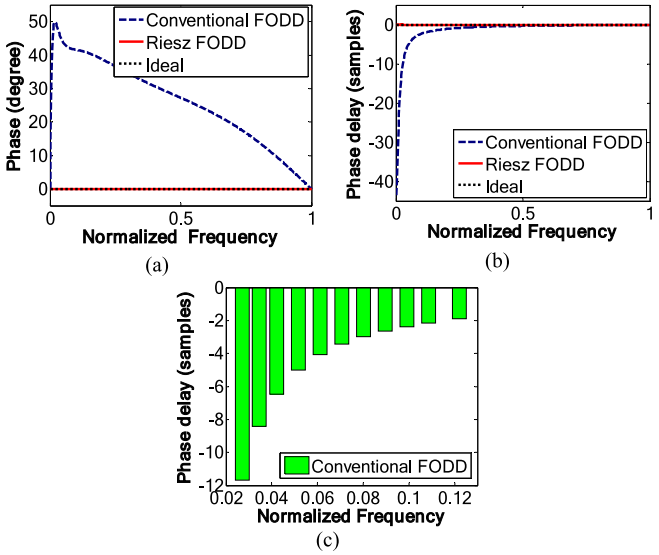

FIGURE 13. Frequency response comparison plots of the ALO-based conventional FODD [19] and the proposed MRFO-based Riesz FODD for $p = 1/2$: (a) phase response, (b) phase delay response, (c) phase delay of conventional fractional order digital differentiator [19] estimated for the normalised frequency range from 0.02 to 0.122.

AFTDB, and TWADB. As shown in Table 8, against each ECG database, the proposed algorithm yields the smallest *FN*, and *FP* beats with the lowest *MTE* in contrast to the reported approaches. The percentage of improvement (*POI*) resulted by using the proposed approach in terms of *FP* (*POI_FP*), and *FN* (*POI_FN*) values over all the reported modern QRS detectors are also illustrated in Table 8. The results confirm the supremacy of the proposed approach compared to high-performance reported QRS detection techniques.

Moreover, compared to the conventional FODD based QRS detector [19], the proposed QRS detector identifies the location of the QRS complex more precisely with respect to database annotations due to the indigenous zero-phase characteristics of the proposed Riesz FODD. It is established in this section through rigorous experiments. Figs. 13(a)–(b) show the phase response and phase-delay response comparison plots between the Ant Lion Optimisation (ALO)-based conventional FODD reported in [19] and the proposed MRFO-based Riesz FODD for $p = 1/2$. From Fig. 13(a) it is clear that the phase of the ALO-based conventional FODD varies from zero to fifty degrees for the entire Nyquist frequency range (NFR).

Similarly, in Fig. 13(b), it can be seen that the phase delay response of the ALO-based conventional FODD varies from zero to forty samples for the complete NFR. However, the phase response (refer to Fig. 13(a)) and the phase delay response (Fig. 13(b)) of the proposed Riesz FODD are almost zero individually. More specifically, for the 5-22 Hz bandpass frequency range (*i.e.*, from 0.02 to 1.22 in the normalised frequency scale), the ALO-based conventional non-zero phase FODD shifts the phase of the differentiated ECG signal from 0 to 12 samples from its unfiltered signal location (refer to Fig. 13(c)). This nonuniform phase delay of non-zero phase conventional FODD is a bottleneck. However, the zero-phase characteristic of the proposed Riesz FODD assists in preserving the feature of the differentiated ECG precisely at the same time instant where they occur in the unfiltered signal.

This unique feature of the proposed Riesz FODD assists in identifying the location of the QRS complex more precisely with respect to the database annotations compared to the conventional ALO-based FODD.

The precise QRS detection ability of the proposed MRFO-Riesz based QRS detector is studied by estimating the *MTE* (ms) between the identified QRS location and the database annotations. The results are compared with the estimated *MTE* of ALO-conventional FODD based QRS detector [19]. As the *MTE* between the detected QRS position and database annotation is not given in [19], the same is estimated in this study by replacing the proposed MRFO-based Riesz FODD by the ALO-based conventional FODD in the feature signal generation stage of the proposed QRS complex detector in Fig. 2. The signal wise summary of the *MTE* of the conventional ALO-based FODD (MTE_{CFODD}) and the proposed MRFO-based Riesz FODD (MTE_{RFODD}) resulted in MITDB ECG signals are shown in Table 9. For all the 48 MITDB ECG signals, the overall *MTE* obtained by the proposed approach is 0.851 ms compared to the *MTE* value of 2.284 ms found by the conventional FODD based approach (refer to Table 8). Thus, by adopting the proposed QRS detector, the *MTE* between the detected QRS position and the database annotation for the MITDB ECG signals is reduced by 63% $(= (2.284 - 0.851)/2.284)$. Similarly,

TABLE 9. MTE obtained against MITDB ECG signals.

ECG	MTE_{CFODD}	MTE_{RFODD}	ECG	MTE_{CFODD}	MTE_{RFODD}
			201	6.52	1.72
100	0.52	0.32	202	0.55	0.06
101	0.51	0.21	203	0.21	0.02
102	1.01	0.32	205	0.24	0.11
103	0.26	0.12	207	0.33	0.16
104	2.11	1.33	208	4.12	1.22
105	2.24	0.82	209	0.85	0.31
106	0.16	0.05	210	0.48	0.22
107	3.03	1.13	212	0.56	0.17
108	11.1	6.63	213	0.84	0.44
109	0.42	0.26	214	1.75	0.59
111	0.82	0.48	215	0.64	0.22
112	0.41	0.31	217	2.63	0.68
113	0.33	0.12	219	13.56	2.21
114	2.22	1.11	220	0.48	0.12
115	0.24	0.11	221	1.89	1.02
116	6.62	2.75	222	0.82	0.36
117	3.01	1.23	223	0.42	0.22
118	0.2	0.1	228	1.98	0.75
119	8.12	3.25	230	0.1	0
121	0.53	0.22	231	0.34	0.14
122	0.12	0.04	232	0.11	0
123	1.45	0.72	233	4.15	1.05
124	0.86	0.34	234	0.22	0
200	19.55	7.12	**Total**	**2.284**	**0.851**

for the EDB, NSTDB, SVDB, AFTDB, and TWADB ECG signals, the lowest *MTE* values are obtained by the proposed QRS detector compared to advanced QRS detectors (refer to Table 8).

VII. CONCLUSION

In this article, recently developed MRFO algorithm along with benchmark LS, CVXO, ABC, and FPA techniques are applied to design zero-phase response Riesz FODD. The exhaustive experimental analysis elects the MRFO algorithm to consistently attain the optimal magnitude (MAME of -12.7742 dB) and just about zero-phase (MPE of 2.9757E-014 degree) responses in the complete Nyquist range. Due to space limitation, the optimal sets of the coefficients of the designed Riesz FODDs are not included in this manuscript. However, these could be supplied to the interested readers by the corresponding author on request.

The zero-phase and optimal magnitude characteristics help to induce QRS related feature signal robustly for a wide diversity of ECG morphology. Hence, a sweeping improvement in the performance of the QRS detector has been noticed when the proposed MRFO-based zero-phase Riesz FODD acts as an essential part of the pre-processor. The enhanced QRS detection performance metrics by the proposed technique is only due to the robust and precise feature signal generation ability of the proposed zero-phase response Riesz FODD, unlike conventional differentiators. This makes the proposed MRFO-based Riesz FODD as the most suitable substitute for pre-processing the ECG signal for the QRS complex detection application. In the future scope of work, a 2-D Riesz FODD could be realised to sharpen the digital image.

REFERENCES

[1] S. K. Berkaya, A. K. Uysal, E. S. Gunal, S. Ergin, S. Gunal, and M. B. Gulmezoglu, "A survey on ECG analysis," *Biomed. Signal Process. Control*, vol. 43, pp. 216–235, May 2018.

[2] J. P. Martínez, R. Almeida, S. Olmos, A. P. Rocha, and P. Laguna, "A wavelet-based ECG delineator: Evaluation on standard databases," *IEEE Trans. Biomed. Eng.*, vol. 51, no. 4, pp. 570–581, Apr. 2004.

[3] C. J. Deepu and Y. Lian, "A joint QRS detection and data compression scheme for wearable sensors," *IEEE Trans. Biomed. Eng.*, vol. 62, no. 1, pp. 165–175, Jan. 2015.

[4] A. K. Dohare, V. Kumar, and R. Kumar, "An efficient new method for the detection of QRS in the electrocardiogram," *Comput. Electr. Eng.*, vol. 40, no. 5, pp. 1717–1730, 2014.

[5] Z. Hou, Y. Dong, J. Xiang, X. Li, and B. Yang, "A real-time QRS detection method based on phase portraits and box-scoring calculation," *IEEE Sensors J.*, vol. 18, no. 9, pp. 3694–3702, May 2018.

[6] X. Tang, Q. Hu, and W. Tang, "A real-time QRS detection system with PR/RT interval and ST-segment measurements for wearable ECG sensors using parallel delta modulators," *IEEE Trans. Biomed. Circuits Syst.*, vol. 12, no. 4, pp. 751–761, Aug. 2018.

[7] S. Yazdani, S. Fallet, and J. M. Vesin, "A novel short-term event extraction algorithm for biomedical signals," *IEEE Trans. Biomed. Eng.*, vol. 65, no. 4, pp. 754–762, Apr. 2018.

[8] T. Sharma and K. K. Sharma, "QRS complex detection in ECG signals using locally adaptive weighted total variation denoising," *Comput. Biol. Med.*, vol. 87, pp. 187–199, Aug. 2017.

[9] D. Pandit, L. Zhang, C. Liu, S. Chattopadhyay, N. Aslam, and C. P. Lim, "A lightweight QRS detector for single lead ECG signals using a max-min difference algorithm," *Comput. Methods Programs Biomed.*, vol. 144, pp. 61–75, Jun. 2017.

[10] M. Elgendi, "Fast QRS detection with an optimised knowledge-based method: Evaluation on 11 standard ECG databases," *PLoS One*, vol. 8, no. 9, pp. 1–18, 2013.

[11] A. Burguera, "Fast QRS detection and ECG compression based on signal structural analysis," *IEEE J. Biomed. Health Inform.*, vol. 23, no. 1, pp. 123–131, Jan. 2018.

[12] S. Choi, M. Adnane, G.-J. Lee, H. Jang, Z. Jiang, and H.-K. Park, "Development of ECG beat segmentation method by combining low-pass filter and irregular R-R interval strategy," *Expert Syst. Appl.*, vol. 37, no. 7, pp. 5208–5218, 2010.

[13] D. Benitez, P. A. Gaydecki, A. Zaidi, and A. P. Fitzpatrick, "The use of the Hilbert transform in ECG signal analysis," *Comput. Biol. Med.*, vol. 31, no. 5, pp. 399–406, 2001.

[14] C. Nayak, S. K. Saha, R. Kar, and D. Mandal, "An optimally designed digital differentiator based pre-processor for R-peak detection in electrocardiogram signal," *Biomed. Signal Process. Control*, vol. 49, pp. 440–464, Mar. 2019.

[15] O. Yakut and E. D. Bolat, "An improved QRS complex detection method having a low computational load," *Biomed. Signal Process. Control*, vol. 42, pp. 230–241, Apr. 2018.

[16] H. Khamis, R. Weiss, Y. Xie, C. W. Chang, N. H. Lovell, and S. J. Redmond, "QRS detection algorithm for telehealth electrocardiogram recordings," *IEEE Trans. Biomed. Eng.*, vol. 63, no. 7, pp. 1377–1388, Jul. 2016.

[17] M. Benmalek and A. Charef, "Digital fractional order operators for R-wave detection in electrocardiogram signal," *IET Signal Process.*, vol. 3, no. 5, pp. 381–391, Sep. 2009.

[18] Y. Ferdi, J. P. Herbeuval, A. Charef, and B. Boucheham, "R wave detection using fractional digital differentiation," *ITBM-RBM*, vol. 24, nos. 5–6, pp. 273–280, 2000.

[19] C. Nayak, S. K. Saha, R. Kar, and D. Mandal, "An efficient and robust digital fractional order differentiator based ECG pre-processor design for QRS detection," *IEEE Trans. Biomed. Circuits Syst.*, vol. 13, no. 4, pp. 682–696, Aug. 2019.

[20] B. T. Krishna, "Studies on fractional order differentiators and integrators: A survey," *Signal Process.*, vol. 91, no. 3, pp. 386–426, Mar. 2011.

[21] C.-C. Tseng and S.-L. Lee, "Design of digital Riesz fractional-order differentiator," *Signal Process.*, vol. 102, pp. 32–45, Sep. 2014.

[22] M. Kumar, T. K. Rawat, R. Anand, R. Karwayun, and A. Jain, "Design of Riesz fractional order differentiator using discrete sine transform," in *Proc. IEEE 3rd Int. Conf. Signal Process. Integr. Netw. (SPIN)*, Noida, India, Sep. 2016, pp. 702–706.

[23] C.-C. Tseng and S.-L. Lee, "Digital image sharpening using Riesz fractional order derivative and discrete Hartley transform," in *Proc. IEEE Asia Pacific Conf. Circuits Syst.*, Ishigaki, Japan, Nov. 2014, pp. 483–486.
[24] A. Kaur, S. Kumar, A. Agarwal, and R. Agarwal, "An efficient R-peak detection using Riesz fractional-order digital differentiator," *Circuits Syst. Signal Process.*, vol. 39, no. 4, pp. 1965–1987, 2020.
[25] W. Zhao, Z. Zhang, and L. Wang, "Manta ray foraging optimisation: An effective bio-inspired optimiser for engineering applications," *Eng. Appl. Artif. Intell.*, vol. 87, pp. 1–25, Jan. 2020.
[26] T. W. Parks and C. S. Burrus, *Digital Filter Design*. Hoboken, NJ, USA: Wiley, 1987, pp. 54–83.
[27] M. Grant and S. Boyd. *CVX: MATLAB Software for Disciplined Convex Programming*. Accessed: Aug. 15, 2020. [Online]. Available: http://cvxr.com/cvx/
[28] D. Karaboga and B. Basturk, "A powerful and efficient algorithm for numerical function optimisation: Artificial bee colony (ABC) algorithm," *J. Glob. Optim.*, vol. 39, no. 3, pp. 459–471, 2007.
[29] X. S. Yang, "Flower pollination algorithm for global optimization," in *Unconventional Computation and Natural Computation*, J. Durand-Lose and N. Jonoska, Eds. Berlin, Germany: Springer, 2012, pp. 240–249.
[30] N. Karaboga and F. Latifoglu, "Elimination of noise on transcranial Doppler signal using IIR filters designed with artificial bee colony—ABC-algorithm," *Digit. Signal Process.*, vol. 23, no. 3, pp. 1051–1058, 2013.
[31] J. P. Ram and N. Rajasekar, "A novel flower pollination based global maximum power point method for solar maximum power point tracking," *IEEE Trans. Power Electron.*, vol. 32, no. 11, pp. 8486–8499, Nov. 2017.
[32] C.-C. Tseng and S.-L. Lee, "Design of matrix fractional order differentiators," *Signal Process.*, vol. 111, pp. 73–88, Jun. 2015.
[33] D. C. Montgomery and G. C. Runger, *Applied Statistics and Probability for Engineers*, 3rd ed. New York, NY, USA: Wiley, 2003.
[34] A. L. Goldberger *et al.*, "PhysioBank, PhysioToolkit, and PhysioNet components of a new research resource for complex physiologic signals," *Circulation*, vol. 101, no. 23, pp. e215–e220, 2000.

CHANDAN NAYAK received the B.Tech. degree in E&I Engineering, and the M.Tech. degree in ECE from the Biju Patnaik University of Technology, Odisha, Rourkela, India, in 2007 and 2012, respectively.

He is currently a Senior Research Fellow with the Department of ECE of NIT Raipur, Chhattisgarh, India. He has published five articles in international journals.

SUMAN KUMAR SAHA received the B.Tech. degree in ECE from the Institution of Engineers, India, in 2006, the M.Tech. degree in I&E Engineering from Jadavpur University, India, in 2009, and the Ph.D. degree in ECE from NIT Durgapur, India, in 2014.

He is currently working as Assistant Professor with the Department of ECE of NIT, Raipur, India. He has more than 50 papers published in international journals and conferences.

RAJIB KAR (Senior Member, IEEE) received the B.E. degree in ECE, from REC, Durgapur, India, in 2001, and the M.Tech. and Ph.D. degrees from NIT Durgapur, India, in 2008 and 2011, respectively.

He is currently attached with the Department of ECE, NIT Durgapur, India, as Associate Professor. He has published more than 370 research papers in international journals and conferences.

DURBADAL MANDAL (Member, IEEE) received the B.E. degree in ECE, from REC, Durgapur, India, in 1996. He received the M.Tech. and Ph.D. degrees from NIT, Durgapur, India, in 2008 and 2011, respectively.

He is currently attached with the Department of ECE, NIT Durgapur, India, as Associate Professor. He has published more than 380 research papers in international journals and conferences.